An improved design for a Current Pulse Electrical ResistanceTomography System

E.W. Randall[1], A.J. Wilkinson[2], T.M. Long[2], K.E. Duggin[2], K. H. Hauslaib[2]
[1] Department of Chemical Engineering, University of Cape Town,
Private Bag, Rondebosch, 7701, South Africa
[2] Department of Electrical Engineering, University of Cape Town
E-mail: bill.randall@uct.ac.za

ABSTRACT

The design and application of the UCT current pulse Electrical Resistance Tomography (ERT) system has been reported at previous world congresses and in several journal papers. Performance has been shown to be similar to that of other designs. This paper describes the latest circuit implementations which were developed using open-source design tools. The updated instrument incorporates an embedded PC with a wireless LAN connection allowing multiple units to be controlled from a master PC work station.

The instrument configuration presented provides a viable, easy to implement and low cost solution for tomography measurements in systems where the medium under investigation is predominantly resistive. Typical applications are in minerals processing mixing systems, bubble columns, and slurry pipe-line flow measurements. The system can acquire data at a rate of 400 dual frames/second using the adjacent pairs measuring strategy and display 2D reconstructions in real-time at approximately 20 frames/second. The recorded data sets can be used to determine velocity profiles in slurry pipe-lines using cross-correlation techniques.

Although there have been many publications dealing with the design of sensor electronics and associated software we believe that this is the first publication of a complete system in sufficient detail for the various circuit elements to be replicated. The circuit descriptions of the various modules and details of the associated software are likely to be of interest to engineers engaged in the design of electrical tomography instrumentation. The multiplexing hardware and the acquisition software could in many cases be used with other sensor systems.

A web site will be launched to coincide with WCIPT6 which will present further details of the system, its performance and applications. The authors hope that this will stimulate interest in the current pulse technique and promote further development and application of such systems.

Keywords: Electrical Resistance Tomography, ERT, Current pulse, instrumentation

1 INTRODUCTION

The operating principle and system features of the UCT current pulse ERT instrument has been described by Wilkinson et al (2005, 2006) and it's performance compared to other available systems by Stephenson et al (2007). The system compared favourably to other instrument's in most of the benchmark tests except linearity. The reviewer's conclusion was that the optimum choice of instrument was dependent on the application. The UCT's strong point, among the systems evaluated, was the high frame capture rate and the ability to access the recorded data sets for off line processing. Since working prototypes have been made available they have provided useful information in several minerals processing applications. Long et al (2006, 2007) used data sets from two electrode rings to determine velocity profiles in a slurry pipe-line. Khanal et al (2009) described work done on a hydro cyclone and employed a novel technique of evaluating the data. More recently Sudhakaran et al (2010) employed the instrument to the determination phase distribution in a bubble column and used a novel technique for interpretation of the tomographic data.

This system implementation incorporates an embedded PC which, with the addition of a display and keyboard, makes the system completely self contained and can operate in a stand alone mode by simply connecting a screen, keyboard and mouse. Remote operation is possible using an Ethernet link which may either be cable or wireless. A single master computer can control several remote ERT units. This allows the instruments to be located close to the electrode rings and eliminate long

electrode cable runs which deteriorate performance, particularly in electrically noisy environments. The embedded PC also facilitates the use of the system in process control applications using techniques described by Randall et al (2007).The details of the electronic circuits for the entire design are described with the exception of the commercially available Eagle USB DAQ and the Intel Atom based embedded PC. The various modules could be incorporated in other designs and the data recording system used in systems where data needs to be acquired in groups of 16 points. Some examples will be provided on the web site illustrating how the PC interacts with the ERT hardware and USB DAQ.

2 SYSTEM IMPLEMENTATION

Although the electronic circuits described in this paper are a complete re-design of the UCT ERT hardware referred to above, compatibility with the controlling micro-controller (MCU) code and data acquisition and processing PC software has been retained. This new implementation of the ERT hardware is more compact and better engineered in terms of interconnecting the various modules. Several circuit modifications and improved circuit board layout have resulted in some improvement of the system performance in terms of signal to noise ratio. The MCU which controls the multiplexers, according to a programmed measurement sequence, and performs the current injection and measurement timing, has been replaced by an in house design based on a Freescale GB60 processor. As this version of the system is specifically targeted at dual-plane flow measurements a multiplexer for only two electrode rings was designed achieving a great reduction in complexity and size. Replacing it with the original multiplexing module described by Wilkinson et al (2006) allows the installation of 128 electrodes which can be configured to provide 3D data sets for off line re-construction.

The MCU has an input, which is enabled via the PC user interface (On Line Tomography application (OLT), and can be used to synchronize frame capture with an external event such as the rotation of an impeller in a mixing vessel. This requires some external circuitry to generate a logic pulse from a detector. Circuits are available to generate these trigger pulses from both optical and magnetic detectors.

The overall system configuration is shown in Figure 1 and photographs of the three main circuit boards in Figure 2. Kicad, a cross-platform open source schematic capture and PCB layout program, was used for the design of the circuit boards. A completely functional ERT instrument can be configured from these three circuit boards with the addition of the MCU, a commercially available data acquisition module and a PC. The current PC application software (OLT) can set the operating parameters of the instrument and plot reconstructed images (for the adjacent pairs strategy) and various other graphs in real time. The data sets may be written to files for more rigorous off line processing.

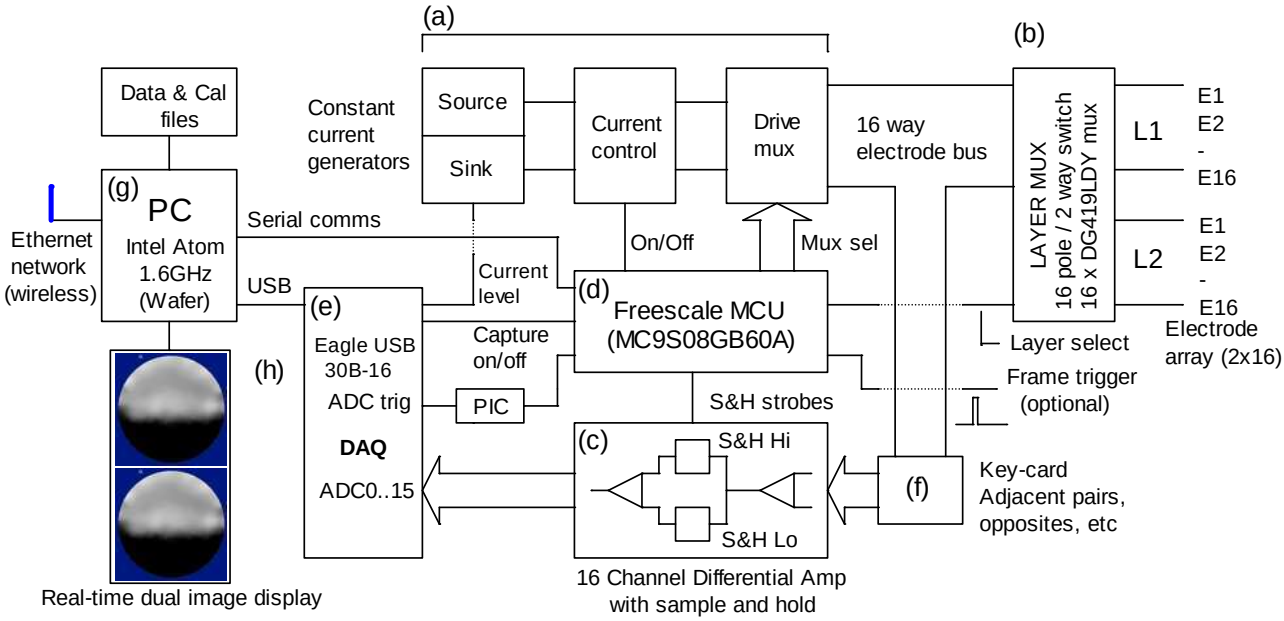

Figure 1. System block diagram: (a) current source and drive mux, (b) 2-layer multiplexer, (c) 16 channel amplifier with sample and hold, (d) MCU, (e) Eagle PC30B16 USB DAQ, (f) key-card, (g) embedded PC (Intel Atom).

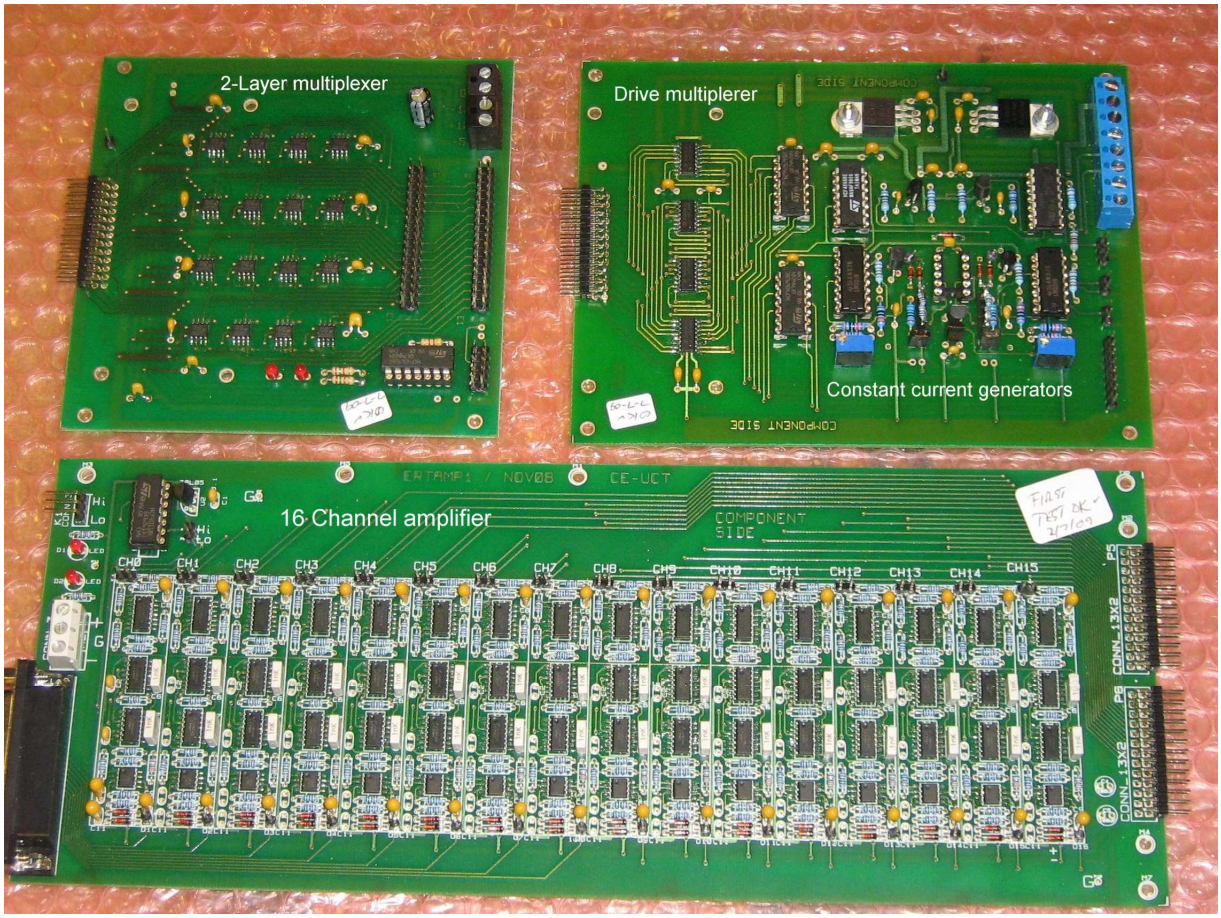

Figure 2. The three circuit boards which provide the basic functionality of the ERT instrument. Designed with Kicad – open source schematic capture and PCB layout software.

2.1 Current source and drive multiplexer

This circuit board performs two functions: (a) the constant current generation, abbreviated circuit shown in Figure 3a which is the basis of the UCT instrument's measuring technique and (b) the drive multiplexer, circuit in Figure 5, which routes the current pulses to the specified electrode pair.

Current pulse timing and electrode selection (via the multiplexers) are performed by the GB60 Freescale micro-controller. Timing constants and electrode selection sequences are downloaded, via serial comms, by the PC to the MCU during system initialization. It should be noted that the current reversal (to achieve the bi-directional pulse which prevents polarization) to a selected electrode pair is achieved by multiplexer switching during the injection sequence. The current level is set by an analogue output from the USB DAQ. Two current ranges (0 to 1mA or 0 to 10mA) are selected by a small mechanical relay which is activated by a switch on the rear panel.

2.1.1 Constant current generators

The current drive circuit consists of two symmetrical sections, one for the current source and the other for the current sink. The current levels are set by a single DAQ analog output of 0 to +5V which provides the control voltages to the current generators via the level shift circuits shown in Figure 3b. Ranges are, Vsource +5 to +10V and Vsink -5 to -10V. To understand the operation of the constant current circuits let us consider the source circuit of op-amp 1. The feedback maintains the voltage at the inverting input equal to that of Vsource applied to the non-inverting input regardless of the load applied to the transistor (Q3) collector. The current is therefore fixed by the range resistor (R1) and Vsource. The current delivered by the circuit is either applied to the selected electrode or bypassed to the -5V rail by switching on FET Q1. When Q1 is on, diode D1 is reversed biased and no current reaches the electrode. This arrangement where the circuit continuously delivers current was found to have superior switching characteristics to that where Vsource is pulsed on and off. The circuit

operation can be verified by applying 2.5V (mid-scale) at the input, which gives +7.5V (Vsource) after level shifting, the feedback ensures that the voltage drop across the range resistor remains constant at 2.5V (i.e. 10-7.5). Constant voltage across the range resistor implies constant current, in the case of the high range (R=500 Ohms) the current is 5mA. The linearity of the circuits are verified by the plots shown in Figure 4.

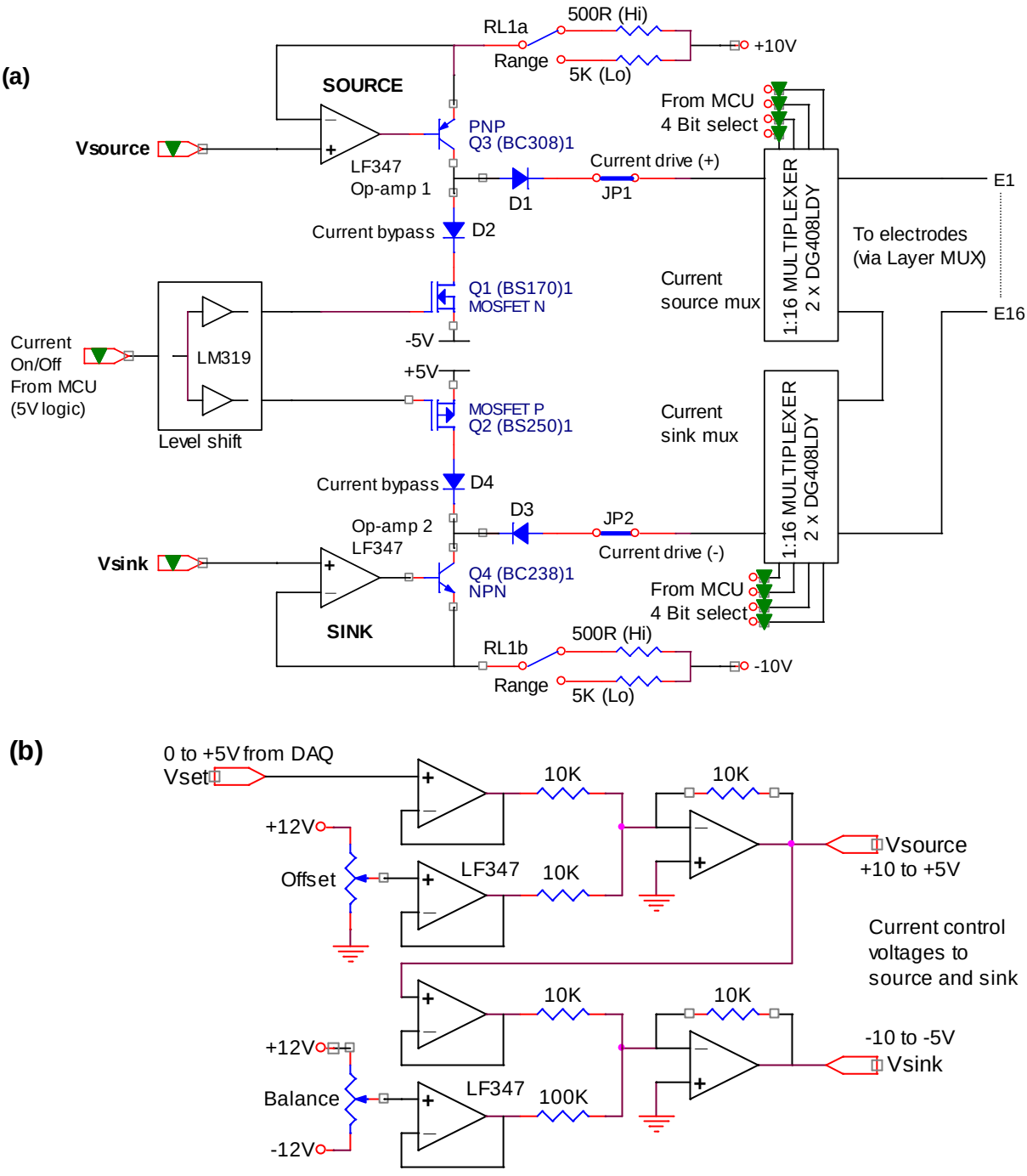

Figure 3. (a) Constant current source/sink circuits and drive multiplexer
(b) Level shift for current control voltages.

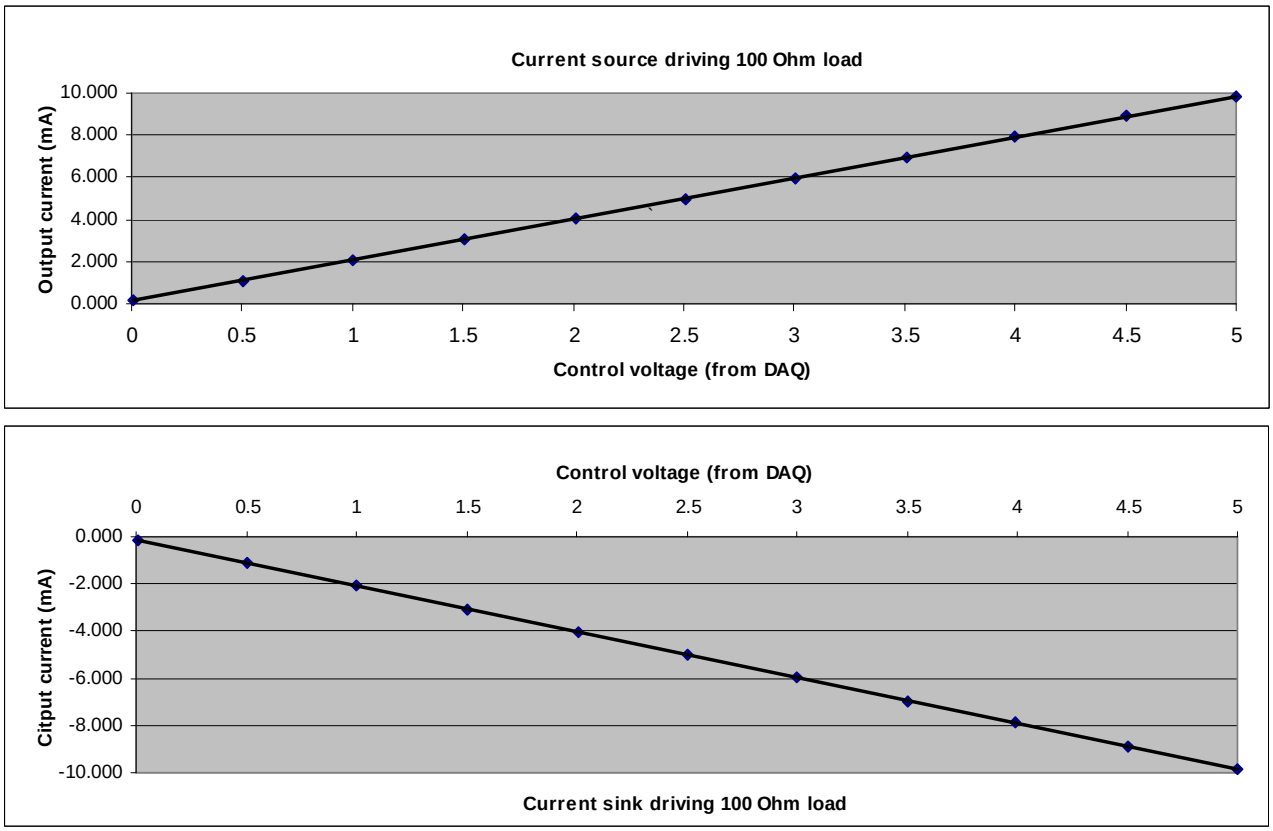

Figure 4. Current source and sink plots verify linearity of the circuits.

2.1.2 Drive multiplexer circuit

Two 1 to 16 way multiplexers are required to route the current source and sink to the selected electrodes. Each of the multiplexers are implemented using a pair of DG408DLY (1 to 8 way) devices. The required device is enabled by the most significant bit of the select inputs. The least 3 significant bits select one of the eight electrodes connected to each device.

Note that the current is delivered to the electrodes via two multiplexers in series, the DG408LDY mentioned above, and also the DG419 in the “layer switching” circuit shown in Figure 10. These devices have nominal “on” resistances of 17 Ohms. As the circuits deliver constant currents up to 10 mA to loads of up to 500 Ohms the resistance of the multiplexer devices is not important although low values are preferable and allow higher current to be delivered to the electrodes.

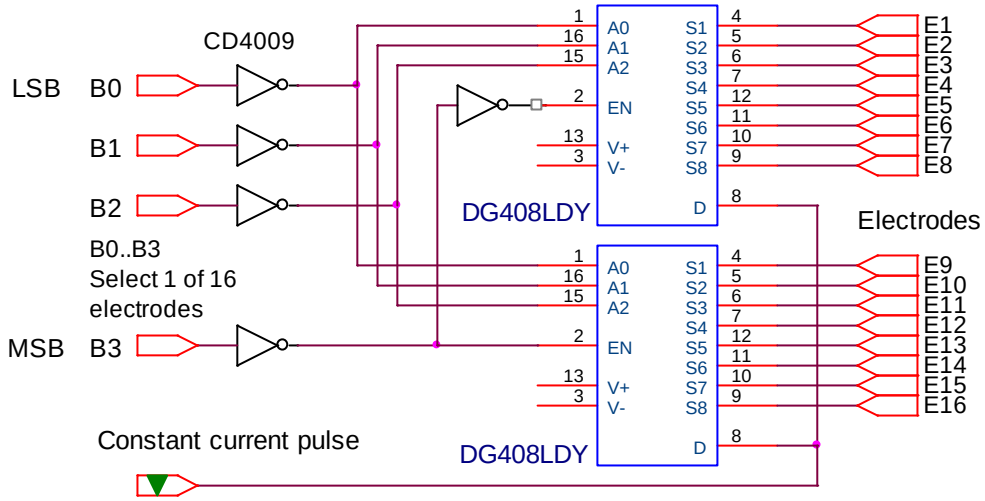

Figure 5. Drive multiplexer schematic (1 of 2), circuit routes current source/sink to selected electrode pair.

To facilitate testing of the multiplexers, they may be isolated from the current generators by removing jumpers J1 and J2 shown in Figure 3. Testing may be done by applying a square wave (amplitude +1V to -1V) to the common input and then cycling the 4 electrode select inputs through the binary sequence 0,0,0,0 to1,1,1,1 and verifying that the square wave appears at each of the 16 outputs (E1 to E16).

2.2 16 Channel differential amplifier

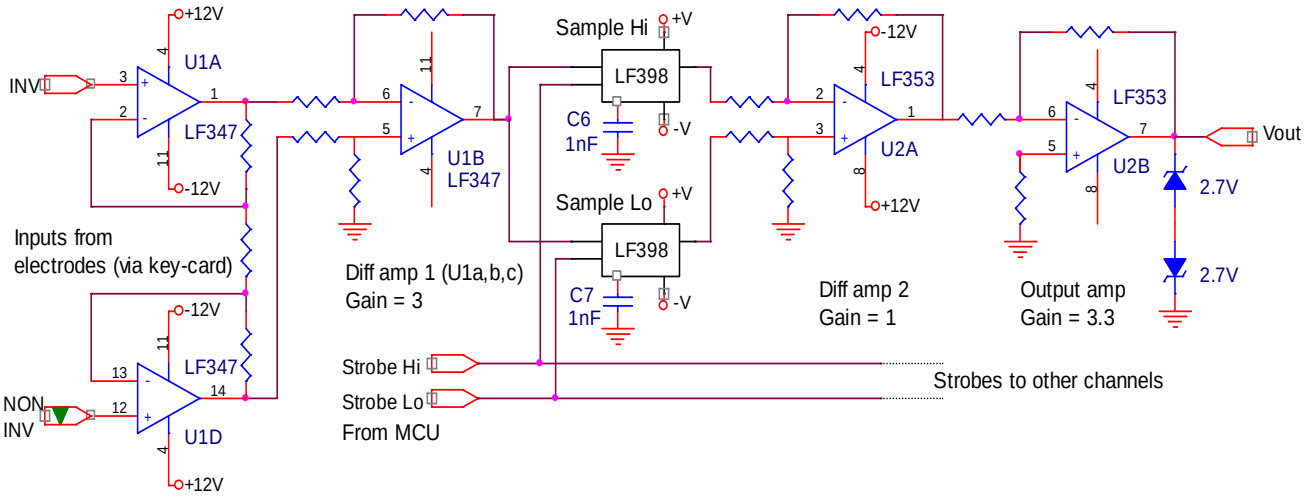

Figure 6. Single amplifier channel with sample and hold (1 of 16)

Table 1. Electrode and amplifier numbering convention for adjacent pairs measuring sequence, connections are made via the "key-card" shown in Figure 1.

Ch 0		Ch 1		Ch 2		Ch 3		Ch 4		Ch 5		Ch 6		Ch 7	
inputs		inputs		inputs		inputs		inputs		inputs		inputs		inputs	
+	-	+	-	+	-	+	-	+	-	+	-	+	-	+	-
E16	E1	E2	E1	E3	E2	E4	E3	E5	E4	E6	E5	E7	E6	E8	E7

Ch 8		Ch 9		Ch 10		Ch 11		Ch 12		Ch 13		Ch 14		Ch 15	
inputs		inputs		inputs		inputs		inputs		inputs		inputs		inputs	
+	-	+	-	+	-	+	-	+	-	+	-	+	-	+	-
E9	E8	E10	E9	E11	E10	E12	E11	E13	E12	E14	E13	E15	E14	E16	E15

Let us consider the operation of a single amplifier channel as shown in the above schematic. The amplitude measurement is made by sampling the voltages from the first differential amplifier during the forward and reverse current injection periods. The current pulse and sample and hold timing, generated by the MCU, is shown in Figure 13 below. The sampled "hi" and "lo" voltages at the LF398 outputs are subtracted by the second differential amplifier (U2A) to give the required amplitude. The final amplifier (U2B) provides some additional gain and the output is digitised by the DAQ and results transferred to the PC via the USB link. The DAQ requires 16 trigger pulses (every 2.5uS) to initiate the reads of the 16 analogue channels. The read triggers are initiated by the MCU after the completion of the sampling and generated by a PIC processor between the MCU and the DAQ. This speeds up the operation as the MCU can reconfigure the multiplexers during the DAQ read operation. The linearity of the measurement system is verified by the plot of input amplitude vs DC output shown in Figure 7 below.

Figure 8 shows the output waveform from an amplifier recorded over a complete frame, i.e. current injection to each of the 16 adjacent electrode pairs. The observation of this wave form at each amplifier, during adjacent pairs data acquisition, is indicative of normal operation of the current

sources, amplifiers and current drive multiplexing system. The wave form is phase shifted on each channel.

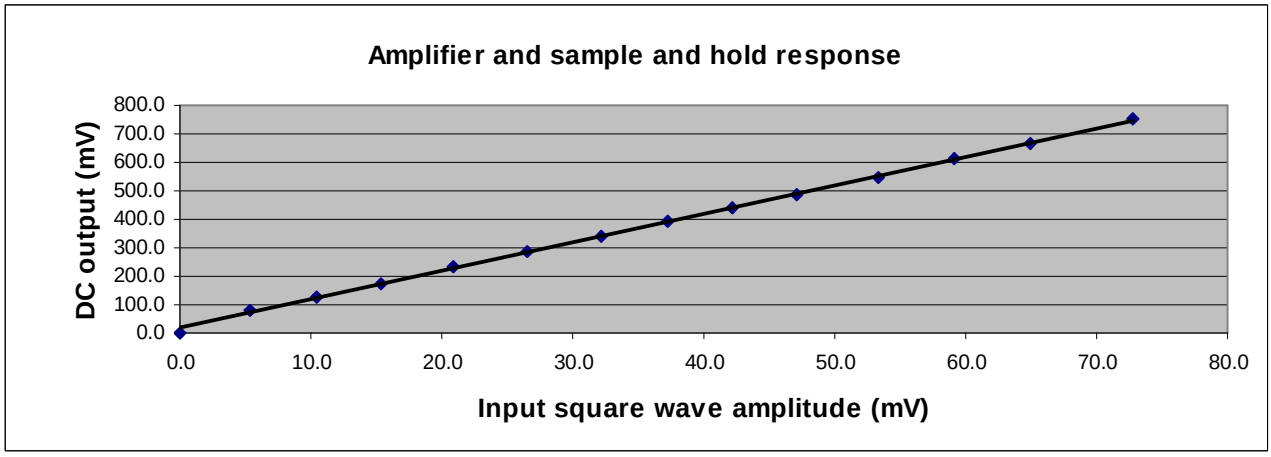

Figure 7. Input vs output verifies linear response of amplifier and sample and hold circuit.

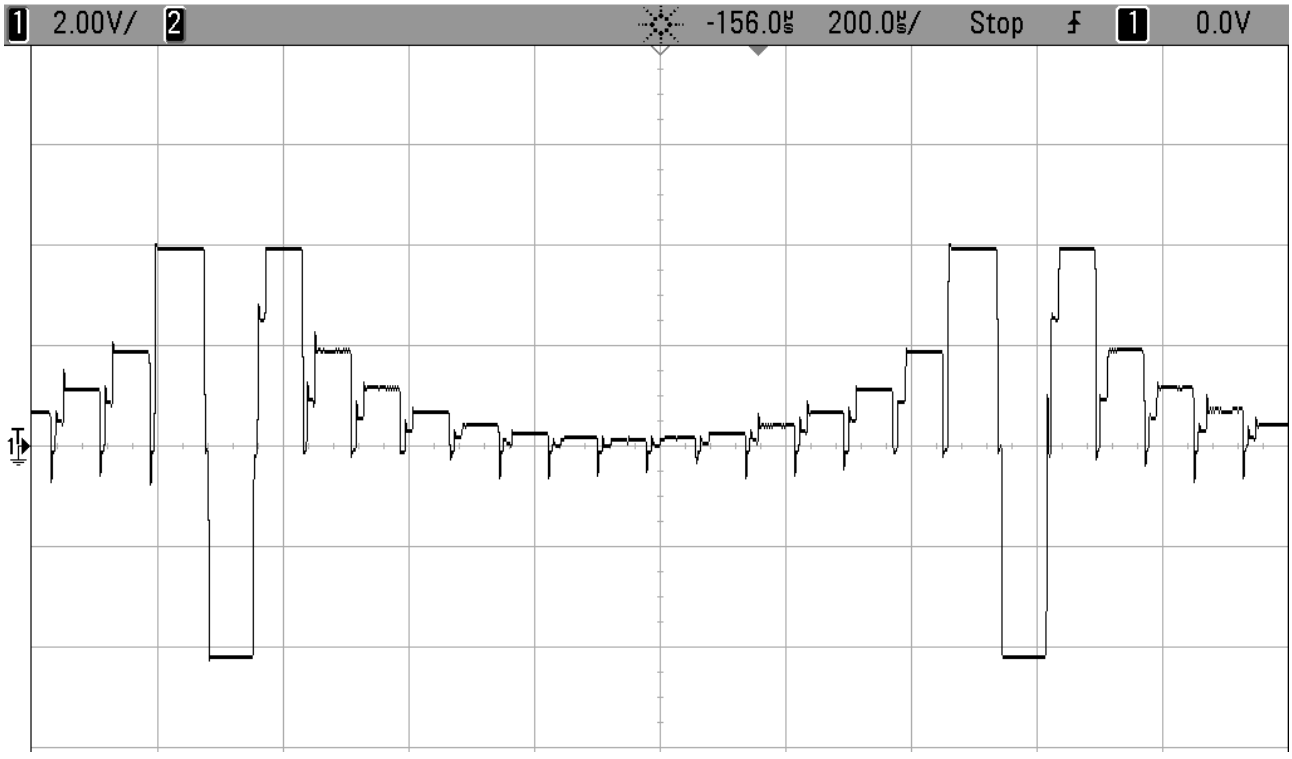

Figure 8. The wave form observed at a single amplifier output (Vout on Figure 6) when acquiring data frames.

The voltages measured between electrodes common to the injection pair are discarded by the PC acquisition software. For each set of 16 ADC readings only the 13 indicated in Table 2 are valid. Each set of valid ADC readings yield the familiar set of 16 “U” curves plotted in Figure 9. This data set is referred to a single “frame” from which the tomogram can be reconstructed. In many applications multiple frames can be averaged to improve the signal to noise ratio before reconstruction. This, however, does not apply when the data is used for velocity determination using cross-correlation techniques as the maximum frame rate is desirable.

The amplifiers are calibrated at system initialization by recording frames (typically 500) with and without current pulses applied. The calibration must be carried out with a homogeneous conductive solution in the measurement vessel. The average frame data sets are stored in a “cal” file from which a 2 point calibration can be performed. A set of calibration constants is computed for each data point in the frame sequence which scales the measured values to coincide with those predicted by the forward model. This procedure compensates for deviations in the amplifier gains and zeros, imperfect electrode geometry as well as inaccuracies in the forward model. The calibration is applied to all subsequently acquired data frames. As all the calibration data is recorded the constants must be re-computed during off-line processing.

Table 2. Valid data points for each of the 16 current injection pairs. Shaded readings are discarded leaving 13 points plotted for each of the 16 “U” curves shown in Figure 9. U curve 1 is ADC2, ADC3, … ADC14, etc.

		Voltage measurement pairs: ADC0 to ADC15															
Inject		E1/16	E2/E1	E3/2	E4/3	E5/4	E6/5	E7/6	E8/7	E9/8	E10/9	E11/10	E12/11	E13/12	E14/13	E15/14	E16/15
E1	E16	ADC0	ADC1	ADC2	ADC3	ADC4	ADC5	ADC6	ADC7	ADC8	ADC9	ADC10	ADC11	ADC12	ADC13	ADC14	ADC15
E2	E1	ADC0	ADC1	ADC2	ADC3	ADC4	ADC5	ADC6	ADC7	ADC8	ADC9	ADC10	ADC11	ADC12	ADC13	ADC14	ADC15
E3	E2	ADC0	ADC1	ADC2	ADC3	ADC4	ADC5	ADC6	ADC7	ADC8	ADC9	ADC10	ADC11	ADC12	ADC13	ADC14	ADC15
E4	E3	ADC0	ADC1	ADC2	ADC3	ADC4	ADC5	ADC6	ADC7	ADC8	ADC9	ADC10	ADC11	ADC12	ADC13	ADC14	ADC15
E5	E4	ADC0	ADC1	ADC2	ADC3	ADC4	ADC5	ADC6	ADC7	ADC8	ADC9	ADC10	ADC11	ADC12	ADC13	ADC14	ADC15
E6	E5	ADC0	ADC1	ADC2	ADC3	ADC4	ADC5	ADC6	ADC7	ADC8	ADC9	ADC10	ADC11	ADC12	ADC13	ADC14	ADC15
E7	E6	ADC0	ADC1	ADC2	ADC3	ADC4	ADC5	ADC6	ADC7	ADC8	ADC9	ADC10	ADC11	ADC12	ADC13	ADC14	ADC15
E8	E7	ADC0	ADC1	ADC2	ADC3	ADC4	ADC5	ADC6	ADC7	ADC8	ADC9	ADC10	ADC11	ADC12	ADC13	ADC14	ADC15
E9	E8	ADC0	ADC1	ADC2	ADC3	ADC4	ADC5	ADC6	ADC7	ADC8	ADC9	ADC10	ADC11	ADC12	ADC13	ADC14	ADC15
E10	E9	ADC0	ADC1	ADC2	ADC3	ADC4	ADC5	ADC6	ADC7	ADC8	ADC9	ADC10	ADC11	ADC12	ADC13	ADC14	ADC15
E11	E10	ADC0	ADC1	ADC2	ADC3	ADC4	ADC5	ADC6	ADC7	ADC8	ADC9	ADC10	ADC11	ADC12	ADC13	ADC14	ADC15
E12	E11	ADC0	ADC1	ADC2	ADC3	ADC4	ADC5	ADC6	ADC7	ADC8	ADC9	ADC10	ADC11	ADC12	ADC13	ADC14	ADC15
E13	E12	ADC0	ADC1	ADC2	ADC3	ADC4	ADC5	ADC6	ADC7	ADC8	ADC9	ADC10	ADC11	ADC12	ADC13	ADC14	ADC15
E14	E13	ADC0	ADC1	ADC2	ADC3	ADC4	ADC5	ADC6	ADC7	ADC8	ADC9	ADC10	ADC11	ADC12	ADC13	ADC14	ADC15
E15	E14	ADC0	ADC1	ADC2	ADC3	ADC4	ADC5	ADC6	ADC7	ADC8	ADC9	ADC10	ADC11	ADC12	ADC13	ADC14	ADC15
E16	E15	ADC0	ADC1	ADC2	ADC3	ADC4	ADC5	ADC6	ADC7	ADC8	ADC9	ADC10	ADC11	ADC12	ADC13	ADC14	ADC15

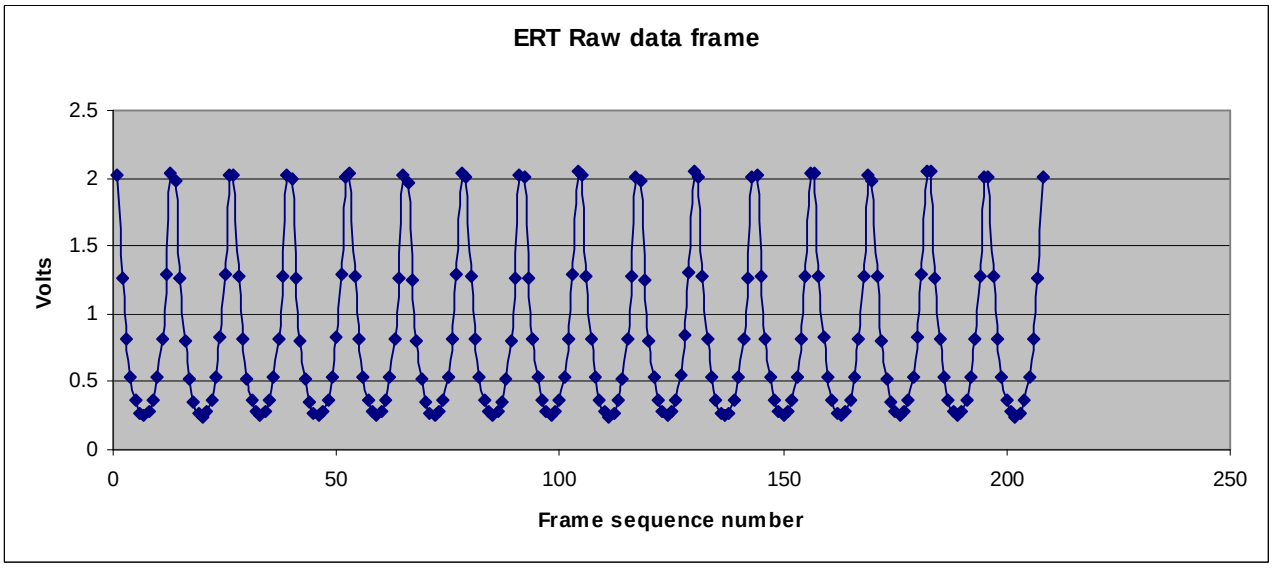

Figure 9. “Typical “U” curve plot representing a single frame of 208 data points from which the reconstructed image is computed. Each “U” is plotted by the 13 useable data points recorded during each of the 16 current injection cycles.

2.3 2-layer multiplexer

The function of this circuit is to connect the required ring of 16 electrodes to the instrument as shown in Figure 1. It performs the function of a 16 pole 2-way switch. A DG419 (1:2 mux), which has a on resistance of 17 Ohms, is used for each of the 16 electrode I/O lines. All 16 devices are switched in parallel by a single logic select input. The connections to the electrodes are bi-directional, outputs during current injection and inputs during voltage measurement.

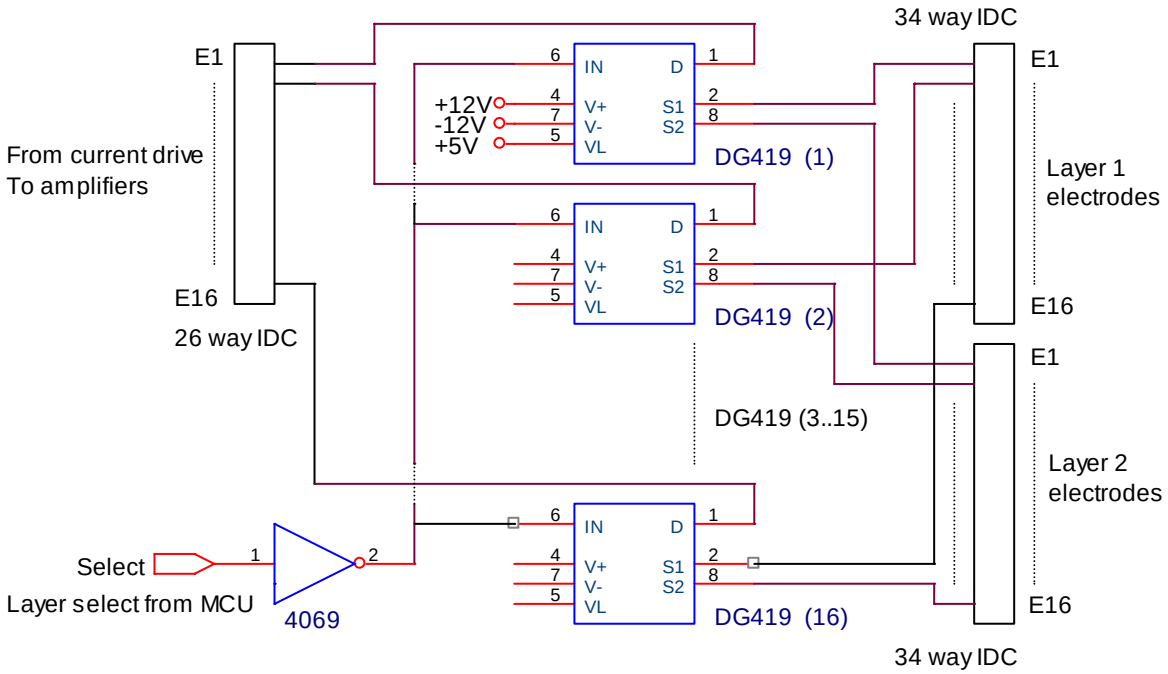

Figure 10. 2-layer multiplexer which has the functionality of a 16-pole / 2 way switch

2.4 Embedded micro-controller (Freescale GB60)

2.4.1 Hardware

The MCU module is implemented on two circuit boards as shown in Figures 11 and 12. The MCU board accommodates the processor, crystal and serial communications driver. The circuit adheres closely to the recommendations of the Freescale application notes and can be used in many instrumentation applications. All 64 pins of the GB60 are taken to connector pins which can plug directly onto an I/O board which is application specific, in this case the board provides buffering of all I/O lines used to interact with the DAQ and ERT hardware.

The MCU system performs two functions while frame capture is in progress. (a) to decode the sequence table and select the current drive multiplexers, and (b) to generate the timing pulses required to inject the current pulses, strobe the sample and hold devices and initiate the reading of the 16 ADC channels on the USB DAQ after each current injection cycle. Figure 13 shows a timing diagram of these signals.

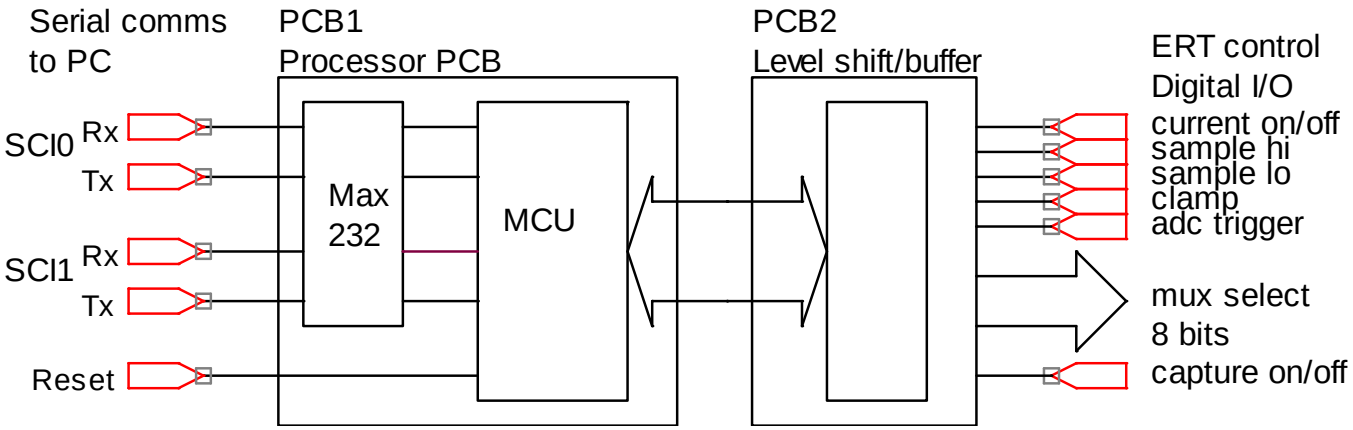

Figure 11. Freescale GB60 MCU system (PCB1) and I/O board (PCB2).

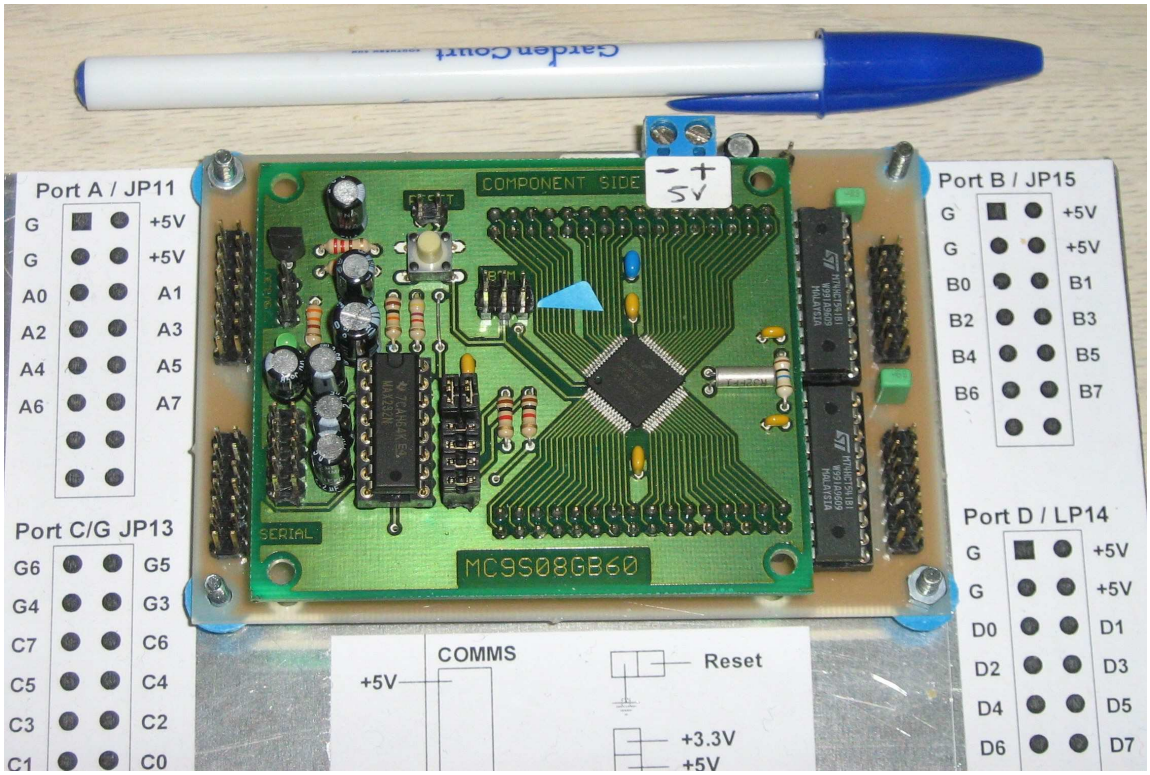

Figure 12. UCT GB60 microcontroller board mounted on I/O board.

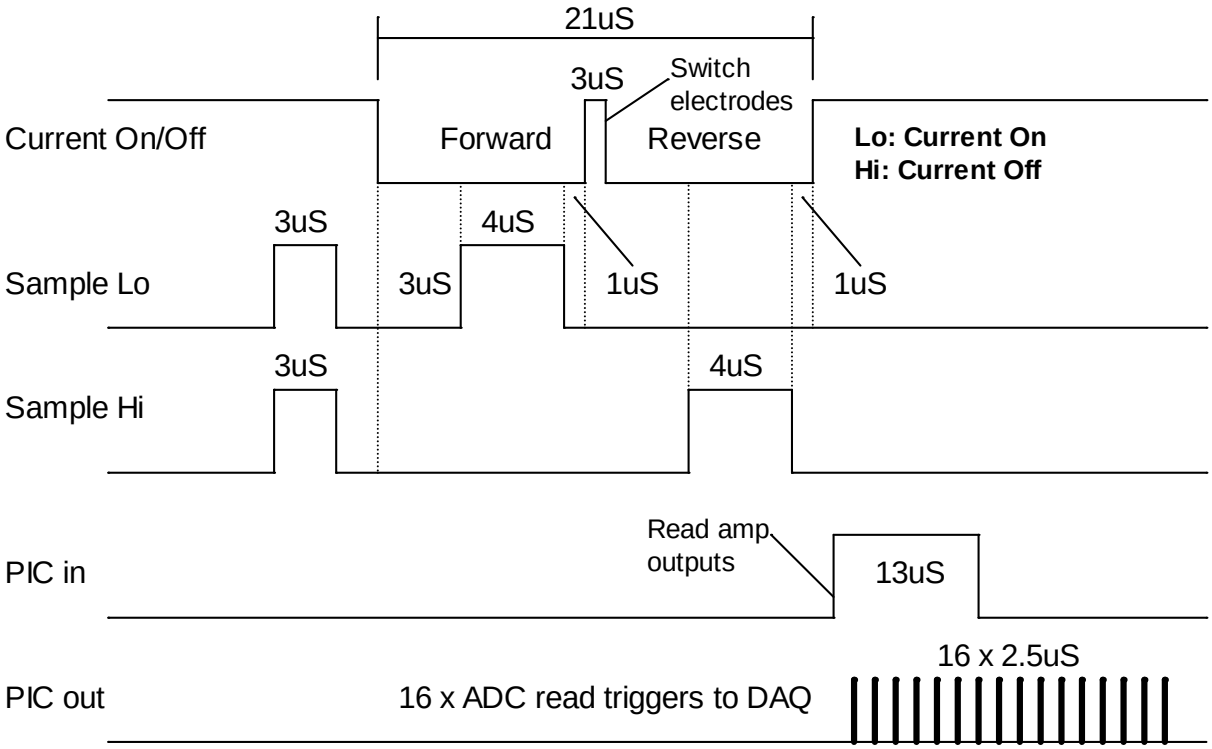

Figure 13. MCU control signals: timing sequence for single current injection cycle and recording of the 16 amplifier outputs. This is repeated 16 times for one frame using adjacent pairs strategy.

2.4.2 Software

The code for the GB60 was written using the Codewarrior development system in conjunction with a PE Micro BDM pod for downloading and debugging the code on the hardware. Assembler language was chosen because of the low level functions performed and the fact that no numerical procedures were required of the MCU.

Two code modules were written:

(a) a serial “downloader” which receives and loads the frame capture code and measurement sequence table into RAM during system initialization. This down-loader is permanently stored in the processors internal flash memory and is executed when reset by the DAQ on command from the controlling PC running OLT. This down-load sequence must be performed after every “reset” of the processor, which is initiated from the PC via the DAQ.

(b) the executable which performs the multiplexing and timing functions (See timing diagram, Figure 13) required for frame capture. Each complete cycle through the sequence table acquires a data frame from which the tomogram can be reconstructed. This code is executed immediately after it is installed in RAM by the down-loader. Execution remains in a wait loop until frame capture is initiated by the PC via the USB DAQ. See “Capture on/off” input to the MCU in Figure 11.

The OLT program on the PC creates an array of bytes to download from two files, the frame capture executable and the sequence table, as shown on the memory map in Figure 14 and file structure diagram in Figure 16. The timing constants at $04A0,1,2 are updated from values entered via the OLT user interface. These constants determine the current pulse widths and sample period timing as shown on the timing diagram inset on the flow sheet and influence the signal to noise ratio achieved.

A flow sheet of the assembler code described above is shown in Figure 15.

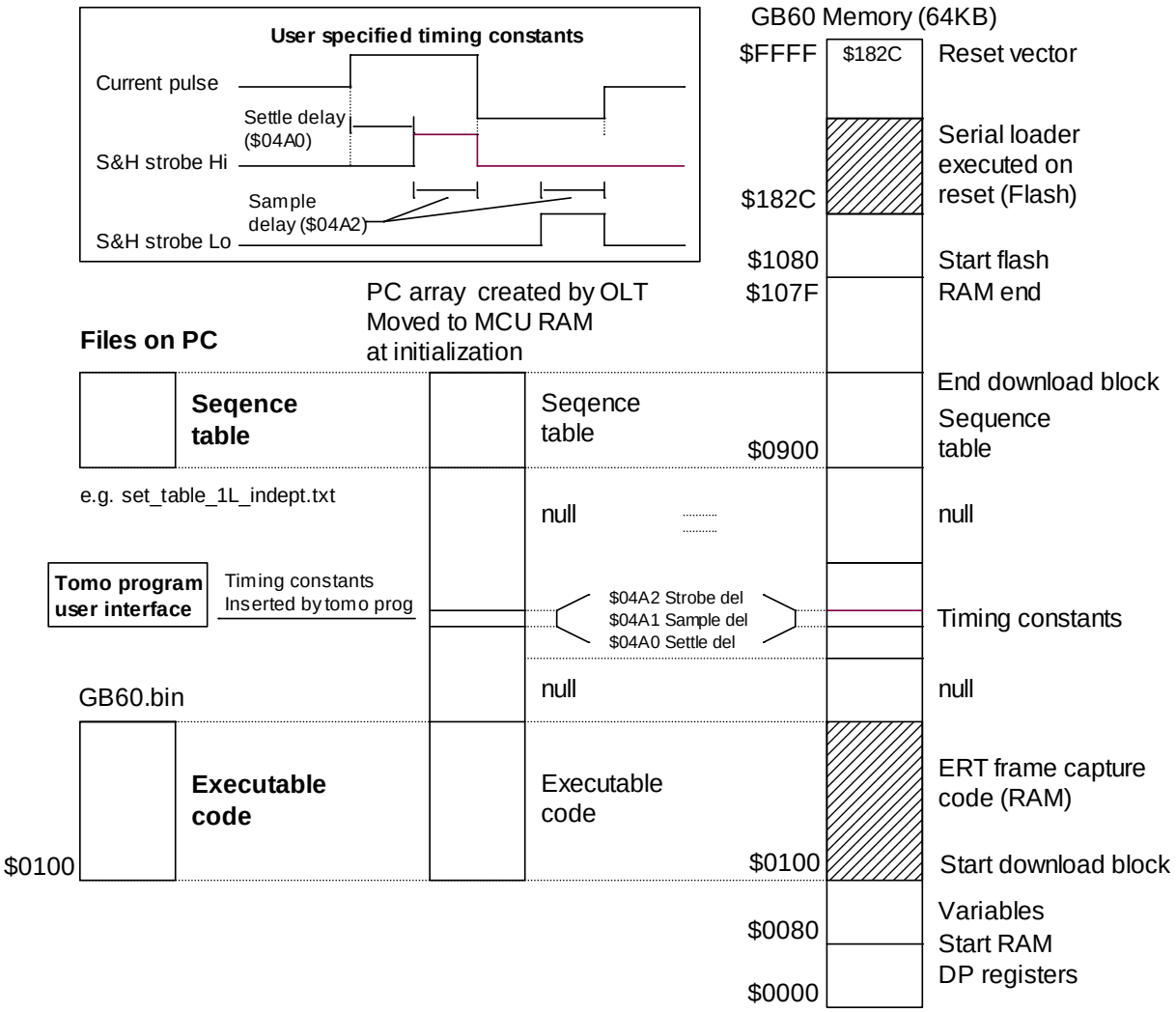

Figure 14. Download array construction and MCU memory map.

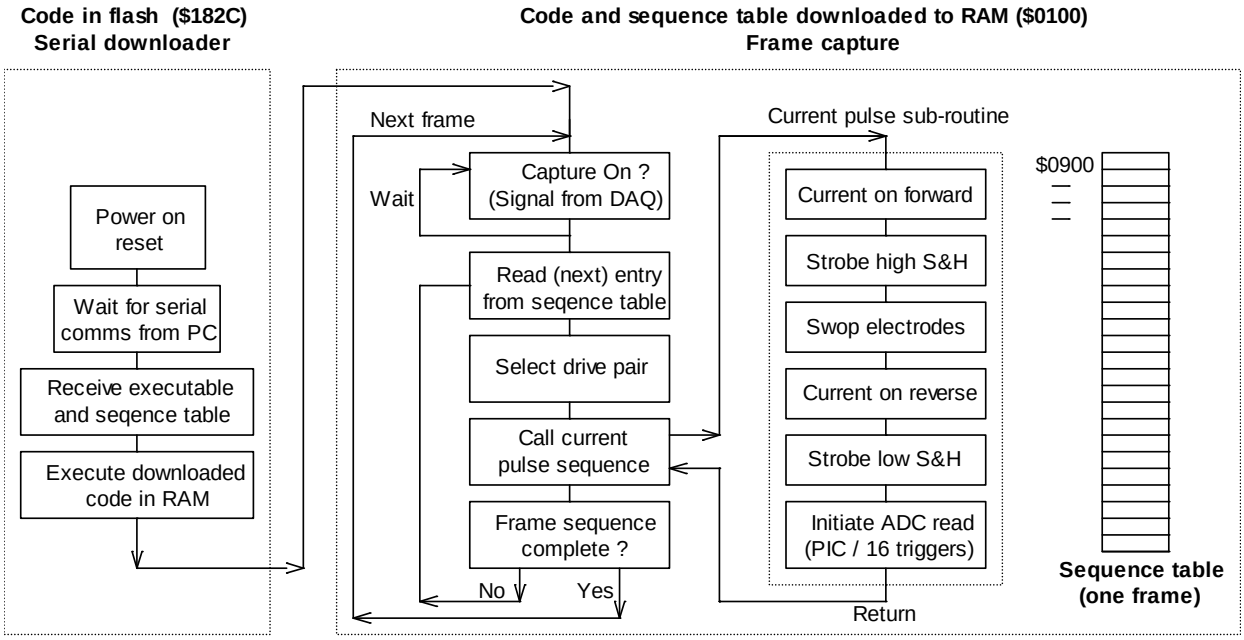

Figure 15. GB60 assembler code flow sheet. Frame capture code is downloaded to RAM by the serial downloader.

2.5 Embedded PC (Intel Atom 1.6GHz)

2.5.1 Hardware

The OLT software was found to perform adequately on small format PC's based on Intel Atom 1.6GHz processors with 1GB RAM installed. Both a Wafer and Asus EeeBox (shown in Figure 16) have been tested, the EeeBox has the advantage of being packaged in a single unit with hard disc and includes a wireless network interface. A Windows-XP license is also included with this unit.

Figure 16. Intel Atom PC's, Wafer (open frame) and Asus EeeBox .

2.5.2 Software

The UCT OLT software which runs the ERT system was written in C++ and uses the cross-platform wxWidgets graphics libraries. It interacts with the GB60 processor via serial comms and the other system hardware via a USB connection to the Eagle USB-30B-16 DAQ. Various operating parameters can be set by the user interface. These include specification of the measurement sequence table and other files used by the on-line reconstruction algorithm. The current version of software's real-time reconstruction algorithm is restricted 2D plots from adjacent pairs data sets. The reconstruction is optimised for speed and spatial resolution is not particularly accurate. The real-time visualization does, however, provide useful information to the operator and in the case of pipe-line flow tests the reconstruction is a good approximation of the solids distribution across the pipe diameter. Various options can be selected for display, these include several versions of the reconstruction plots as well as data frame and noise graphs. The calibration and data sets can be logged to files for off line processing.

The input and output files used by OLT are shown in Figure 17 below and have the following functions:

(a) The "MCU executable file" contains the multiplexing and timing code downloaded to the GB60 processor.

(b) The "sequence file" specifies the current injection and measurement sequence. It is decoded by the executable referred to in (a).
The structure of the sequence table has been described by Wilkinson (2006).

(c) The "mesh file" specifies the geometry of the finite elements mesh used by the reconstruction algorithm and must correspond to the pre-computed file referred to below.

(d) The “pre-computed file” contains the pre-computed matrix used for the single step reconstruction algorithm and significantly speeds up the computation.

(e) The “calibration file” contains the current off and on frame data sets used to perform the 2 point calibration.

(f) The “frame data file” contains the data sets for off line processing. Matlab scripts are available for extracting the data from these and can been used to format the data frames for reconstruction by EIDORS functions, Polydorides et al (2002) and Adler (2006).

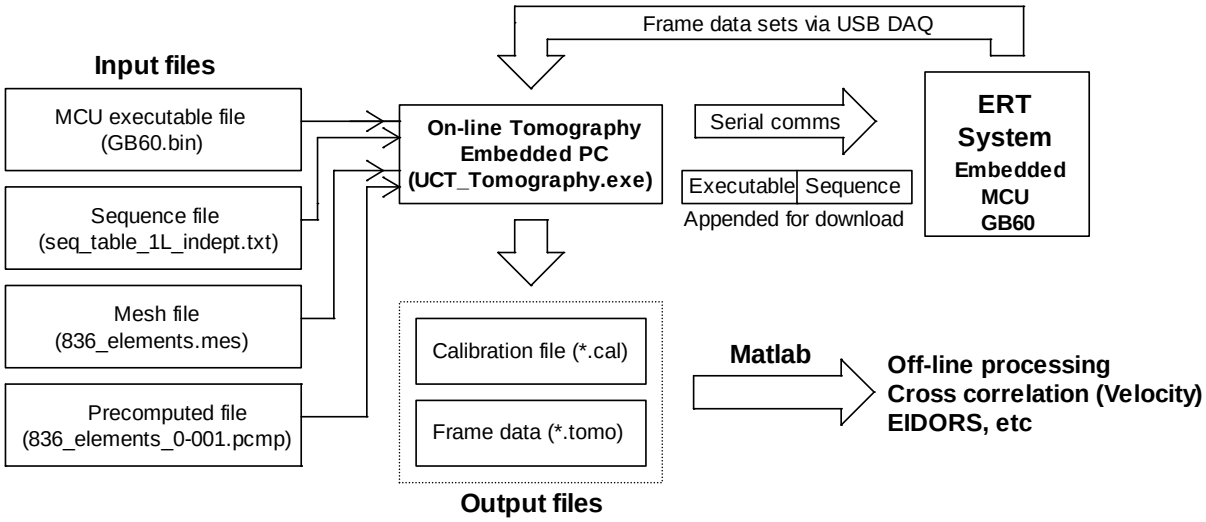

Figure 17. Input and output files used by On-Line Tomography application.

2.6 System configurations

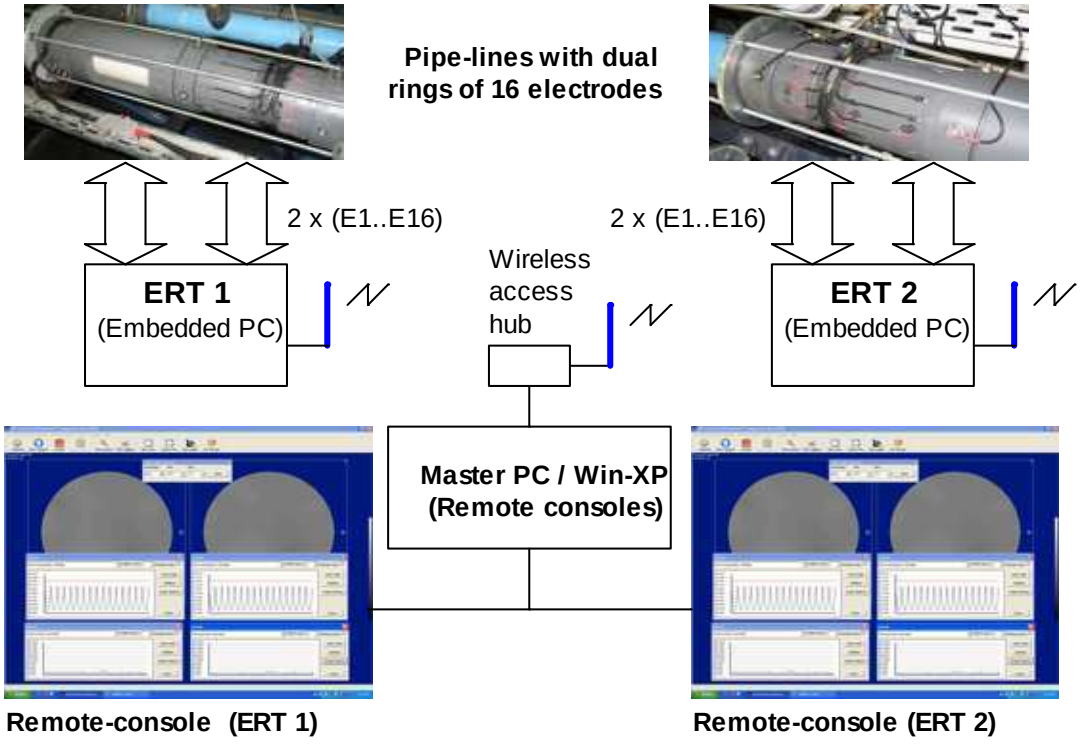

Figure 18. System configuration for monitoring two dual electrode rings on a slurry pipe-line

Many permutations of the described hardware can be assembled to accommodate various experimental requirements. These range from basic systems with a single ring of 16 electrodes (no layer multiplexer required) to multiple ERT instruments controlled remotely using a wireless network. The configuration of such a distributed system is shown in Figure 18. Remote operation of the OLT software on the embedded PC, using the Windows Remote Console using a 100 Mb/sec Ethernet link shows no perceptible degradation in performance as viewed on the remote station. The VNC remote control software was also tested but screen updates were not as smooth as with Windows Remote Console.

2.7 Verification tests

The data presented below verifies the operation of the described ERT hardware. All tests were conducted in a 220mm diameter ERT measurement tank filled with saline solution and various phantoms and bubble plumes introduced. A typical 16 electrode adjacent pairs data frame plot (for a homogeneous solution) is shown in Figure 19 and the corresponding the noise plot is shown in Figure 20. This shows an average standard deviation of approximately 1.5mV for data recorded at 800 frames/second.

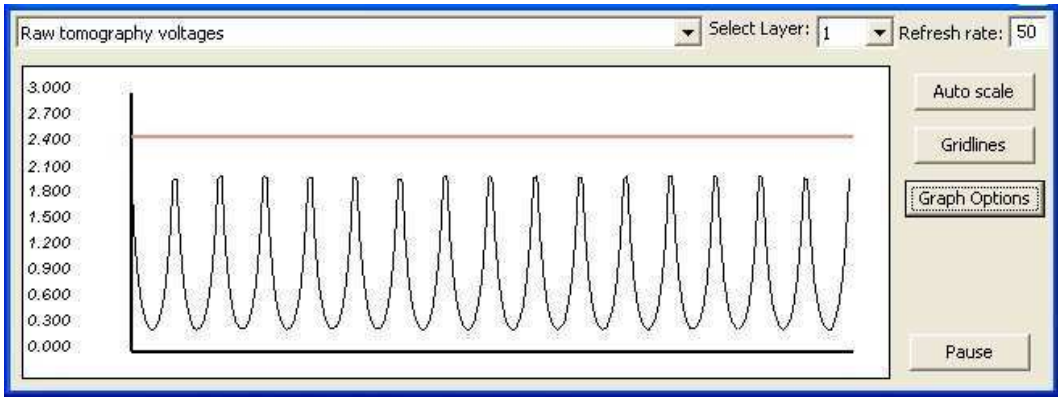

Figure 19. Uncalibrated data frame recorded for a homogenous conductive solution using adjacent pairs current injections and measurements.

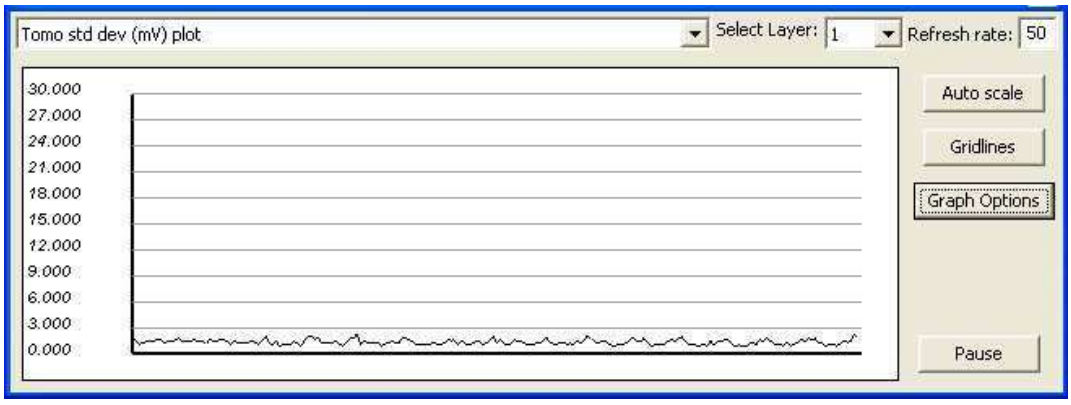

Figure 20. Standard deviation of noise calculated for 100 consecutive frames, one of which is shown above in Figure 19.

Figure 21 shows images reconstructed by the OLT software for an insulating phantom. The grey scale range may be set to represent a specified conductivity range, e.g. a grey scale range of 10% implies a change from black to white for conductivity change of 10%. Decreasing the range enables physically smaller objects or disturbances with conductivity only slightly different (e.g. a bubble stream) from the solution conductivity to be resolved.

(A) and (B) show the effect of decreasing the grey scale range from 40% to 20% for a 25mm (9.5% of tank diameter) insulating rod located off centre in the measuring tank. (C) and (D) are images of a 12mm (5.5% of tank diameter) insulating rod at the centre of the tank. The narrower range allows the smaller phantom to be detected. The adjacent pairs strategy gives poor sensitivity at the centre whereas opposite pairs current injection would significantly improve the resolution in this region.

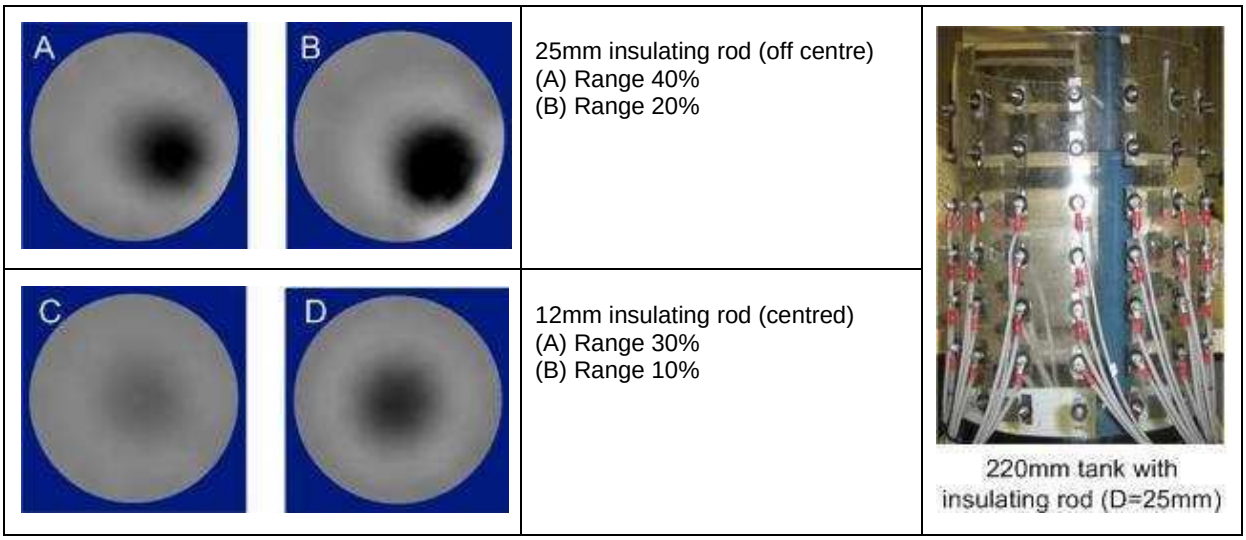

Figure 21. Images of insulating rod in saline solution

Figure 22 shows images from tests on bubble streams in the ERT measuring tank. (E) and (F) show an increase in size of the plume as air flow to the air sparger is increased. (G) and (H) show the effect of decreasing the conductivity range of the plot. The inherent noise over the tomogram is less than 1% and changes in conductivity in the order of 2% can be detected.

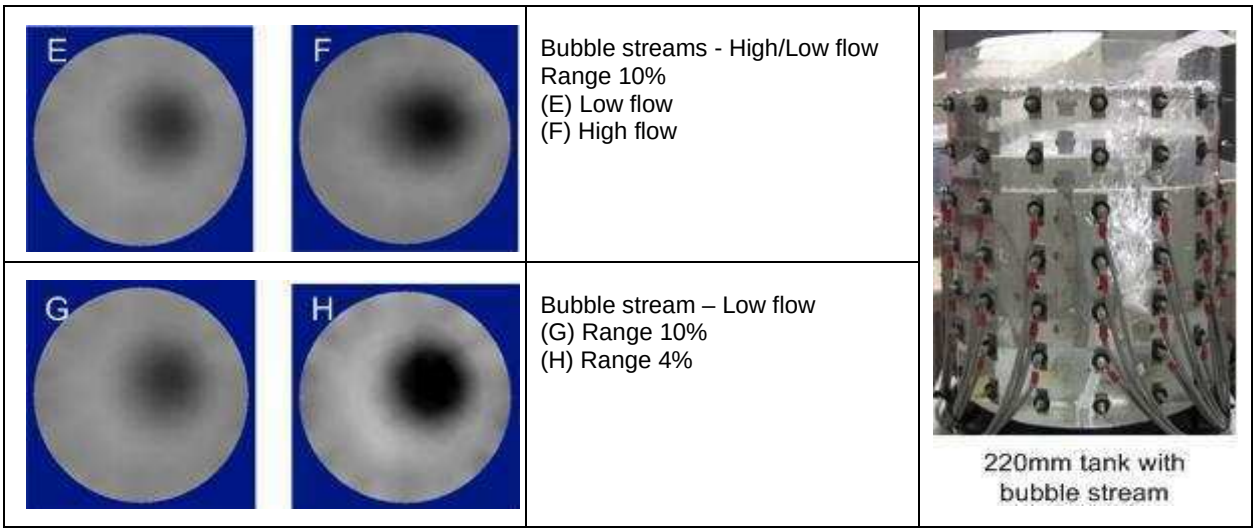

Figure 22. Images of bubbles in saline solution

The reconstructed images were generated by the high speed algorithm embedded in the OLT software used for data acquisition and real-time visualization. The effect of the regularization and grey scale range on the image representation is discussed by Wilkinson et al (2006). Significantly more accurate results can be achieved by off line processing. Currently alternative measurement strategies and reconstruction methods are being investigated using the EIDORS software with the aim of finding optimum techniques for specific experimental conditions.

3 CONCLUSIONS

The current pulse ERT system hardware described is relatively cheap and easy to construct. Performance is acceptable for many applications, particularly in the field of minerals processing. The acquisition speed of 400 dual frames/second is adequate for velocity measurements up to 4 m/s using cross-correlation techniques. Successful correlation is, however, dependent on the size distribution of solid material in the slurry. The current version of the operating software can display 2D reconstructed

images in real-time (at 20 frames/second) and record the data sets for more rigorous off line processing.

More work needs to be done in the area of extracting useful engineering parameters from the tomographic data sets. Khanal (2009) et al have made a contribution to this in their application of least-squares regression modelling to the interpretation of tomographic data acquired by the UCT instrument. Stephenson et al (2008) have reviewed several reconstruction techniques and demonstrated that they give significantly varying results. Adler et al (2006) have drawn attention to the difficulties in solving inverse problems and of advised on how EIDORS can be used to reduce numerical problems in image reconstruction.

The UCT instrument, with full multiplexing system installed, is capable of recording large data sets. The increase in data set size does not, however, necessarily improve the accuracy of the reconstructed image. The optimum measurement strategy and appropriate forward models for specific systems under investigation would be an interesting study. The development of techniques for the interpretation of the recorded data is probably the area of research that is likely to yield more accurate and useful engineering information.

4 ACKNOWLEDGMENTS

The authors would like to thank the following people who have contributed to the project: Andrew Sutherland for his co-operation in access to the pipe-line test facility at the Cape Peninsula University of Technology. To Stephan Stoeckigt for the design of the MCU system and many other students who have contributed to the project and to Graham Inggs for his advice on configuring IP networks. We would also like to thank our colleagues at the University of Queensland (JKMRC), the CSIRO (Kosta Simic), University of Ottawa (Andy Adler), University of Manchester (Trevor York, Bill Lionheart and David Stephenson) and Teltek (Saba Mylvaganam) for their technical and financial support over the course of the project. Thanks are also due to the NRF (South Africa) for various student funding grants to contributing students.

5 NOMENCLATURE

Atom	Intel processor used in PCs
Codewarrior	Software development system for Freescale MCU's
DAQ	Data Acquisition System
ADC	Analogue to Digital Converter
ERT	Electrical Resistance Tomography
EIDORS	Electrical Impedance tomography and Diffuse Optical Reconstruction Software
OLT	On-Line Tomography (UCT Tomography application program)
MCU	Micro Controller Unit
PC	Personal Computer
PCB	Printed Circuit Board
USB	Universal Serial Bus
VNC	Virtual Network Computing, remote access and control software http://www.realvnc.com
wxWidgets	http://www.wxwidgets.org, open source graphics and TCP/IP function libraries
Kicad	http://iut-tice.ujf-grenoble.fr/kicad, open source electronic design and PCB layout software developed by Jean-Pierre Charras, LIS, France

6 REFERENCES

ADLER, A., LIONHEART, R.B. (2006), Users and abuses of EIDORS: An extensible software base for EIT. Physiological Measurement, 27 S25

KHANAL, M., MORRISON, R., (2009) Analysis of electrical resistance tomography (ERT) data using least-squares regression modeling in industrial process tomography,, Meas. Sci. Technol. 20, 045503 (8pp).

LONG, T.M., (2006), An on-line velocity profiling system using Electrical Resistance Tomography, MSc thesis, University of Cape Town.

LONG, T.M., (2007), An on-line velocity profiling system using Electrical Resistance Tomography, In Proc., World Congress of Industrial Process Tomography, Bergen, Norway

POLYDORIDES, N.P., LIONHEART W.R.B., (2002) 'A MATLAB toolkit for three dimensional electrical impedance tomography: A contribution to the EIDORS project', Meas. Sci. Technol. 13, pp. 1871-1883

RANDALL, E.W., LONG, T.M., SALKINDER, J., (2007), System Design for the Control of a Tomography Instrument via an IP link, In Proc., 5th World Congress of Industrial Process Tomography, Bergen, Norway

STEPHENSON, D. R., MANN, R., YORK, T.A., (2008), The sensitivity of reconstructed images and process engineering metrics to key choices in practical electrical impedance tomography, (2008), Meas. Sci. Technol. 19, 094013 (15pp).

STEPHENSON, D. R., YORK, T.A., MANN, R., (2007), Performance and Requirements of Process ERT Instruments. In Proc., 5th World Congress of Industrial Process Tomography, Bergen, Norway

SUDHAKARAN, H., RANDALL E.W., U. RAMDHANI U., RAWATLAL R., (2010), Application of tomography to quantative analysis of phase distribution in bubble column reactors, (2010), WCIPT6, Beijing, China

WILKINSON, A.J., RANDALL, E.W., CILLIERS, J.J., DURRETT, D.R., NAIDOO, T., LONG. T., (2005), A 1000-Measurement Frames/Second ERT Data Capture System with Real-Time Visualization, IEEE Sensors Journal, Volume 5, Number 2., pp 300 – 307

WILKINSON, A.J., RANDALL, E.W., LONG, T.M., COLLINS, A., (2006), The design of an ERT system for 3D data acquisition and a quantitative evaluation of its performance, Meas. Sci. and Technol., 17, pp 2088-2096